Renewable Energy 177 (2021) 209–215

Contents lists available at ScienceDirect

Renewable Energy

journal homepage: www.elsevier.com/locate/renene

Carbons derived from alcohol-treated bacterial cellulose with optimal porosity for Li–O_2 batteries

Wenhai Wang [a], Siavash Khabazian [b], Soledad Roig-Sanchez [a], Anna Laromaine [a], Anna Roig [a], Dino Tonti [a, *]

[a] Institut de Ciència de Materials de Barcelona, ICMAB-CSIC, Campus UAB, 08193, Bellaterra, Spain
[b] Nanomaterials Group, Department of Materials Science and Engineering, Tarbiat Modares University, Tehran, Iran

ARTICLE INFO

Article history:
Received 10 February 2021
Received in revised form
22 April 2021
Accepted 9 May 2021
Available online 26 May 2021

Keywords:
Bacterial cellulose
Solvent exchange
Porous carbons
Electrochemical surface area
Li–O_2 batteries

ABSTRACT

Porous carbons are important cathode materials for metal-air batteries, but the most usual methods to prepare these porous structures are complex and of high cost. We have prepared porous carbons from bacterial cellulose (BC) hydrogels by a simple water-alcohol solvent exchange before carbonization. Alcohol treatment facilitates looser and more open structures than untreated BC, resulting in porous carbon structures with high surface area, appropriate for electrochemical applications. Used as cathodes in lithium-oxygen batteries, the carbon derived from 1-butanol treated BC has excellent discharge capacity (5.6 mA h cm^{-2}) and good cycle life. This work presents a sustainable, straightforward and fast way to prepare porous carbon materials from BC.
© 2021 The Author(s). Published by Elsevier Ltd. This is an open access article under the CC BY license (http://creativecommons.org/licenses/by/4.0/).

1. Introduction

With the development of society, the demand for energy becomes an urgent need. Many aspects of energy-storage technologies have been explored to facilitate the use of sustainable energy sources [1,2]. Among these technologies, Li–O_2 battery has been regarded as one of the most promising, because of its high theoretical energy density of ~3500 Wh kg^{-1} [3]. But there are still numerous issues impeding the utilization of Li–O_2 batteries in practical use [4,5]. Owing to their sluggish kinetics, the oxygen reduction reaction (ORR) and the oxygen evolution reaction (OER) show large overpotentials, low energy and coulombic efficiency [6,7]. The performance of a Li–O_2 battery relies on the reaction between lithium ion and oxygen. A good cathode should allow the diffusion of lithium ions and oxygen, and also favor the reversible Li_2O_2 formation and storage during the process of discharge [8,9]. Porous carbons are the most widely used platform for air cathodes [10,11], as they generally offer good conductivity, light weight, large surface area, tunable porosity, and low cost and abundant, often renewable, sources for its production [12,13].

Bacterial cellulose (BC) is a bio-based polymer produced from a microbial fermentation process [14,15], which is employed in a wide range of applications from health to electronics [16,17]. BC as carbon source has raised great attention, owing it to its sustainability, relative low cost, three-dimensional structure, high surface area and accessible porosity [18,19], which are ideal for electrodes in energy storage devices. As-prepared BC is a hydrogel, thus thermal carbonization requires a drying step. The drying route applied considerably modifies the morphology, surface area and porosity of the BC, therefore it can influence the properties of the resulting carbons [20,21]. In fact, when the gel is dried by simple water evaporation in air at room or oven temperature, the strong capillary forces collapse the pores of the cellulose network, which induces fibril aggregation known as hornification, resulting in a low porosity material. Freeze-drying, spray-drying and supercritical drying are often used to hinder hornification [22,23], increasing the surface area of cellulose and producing porous structures.

Such porous cellulose has been successfully employed to produce carbons with a nanofibrous structure that replicates the nanocellulose network [18,24]. However, the drying methods applied are generally time- and energy-consuming and require expensive facilities than simple oven drying. Therefore these methods do not represent a remarkable advantage over more conventional methods to introduce and control porosity of

* Corresponding author.
E-mail address: dino.t@csic.es (D. Tonti).

https://doi.org/10.1016/j.renene.2021.05.059
0960-1481/© 2021 The Author(s). Published by Elsevier Ltd. This is an open access article under the CC BY license (http://creativecommons.org/licenses/by/4.0/).

biomass-derived carbons, as it is the case of chemical activation by corrosive compounds [25,26], addition of templating agents [27], or hydrothermal synthesis [28]. On the other hand, some authors reported that using compatible solvents with low surface tension, such as alcohols, could relieve the occurrence of a compacted structure's cellulose [29,30].

We show here a facile and low-cost method to prepare porous carbons from food store commercial BC after a simple alcohol treatment. The obtained carbon microstructure is not a replica of the cellulose and suggests some intermediate melting step in the pyrolysis process. Nevertheless, the porosity of carbon derived from alcohol-treated BC is remarkable and used as oxygen cathodes in Li–O_2 batteries showed an outstanding capacity and good cycle life. These results not only show a more economic and sustainable route for the preparation of porous carbons, but the striking variations of carbon porosities and electrochemical performance obtained from the same cellulose modified just by controlling fiber aggregation also provide an interesting insight into the carbonization process.

2. Experimental

2.1. Materials

Bacterial cellulose (BC, Q-Phil Products International), methanol (Scharlau), ethanol (99%, Panreac), 1-propanol (99.7%, Sigma Aldrich), 1-butanol (99.5%, Labkem), 1-hexanol (≥99.9%, Sigma Aldrich), 1-octanol (≥99.9%, Sigma Aldrich), ether (≥99.9%, Sigma Aldrich), acetone (99%, Panreac), Tetraethylene glycol dimethyl ether ether (TEGDME, ≥97.0%, Sigma Aldrich), N-methyl-pyrrolidone (NMP, Sigma Aldrich), lithium triflate (99.95%, Sigma-Aldrich), bis(2-methoxy ethyl)ether (Diethylene glycol dimethyl ether, DEGDME, 99.95%, Sigma-Aldrich), polyvinylidene fluoride (PVDF, Sigma-Aldrich), carbon black (Super P, Timcal), lithium foil (Sigma-Aldrich, 0.4 mm thick), carbon paper (Freudenberg, H2315, 210 μm thick), glass fibre filter (PRAT DUMAS, 270 μm thick).

2.2. Preparation of carbons

BC processing: Food-grade BC was in the form of cubes (approx. size 15 × 15 × 15 mm^3) immersed in sucrose syrup. Cubes were drained and placed in Milli-Q water under stirring for 3 h, this process was repeated twice to remove the absorbed syrup and a final step of 12 h. Then, the BC cubes were autoclaved at 120 °C for 20 min. To replace water with other solvents, one piece of BC was pressed by a Teflon cylinder (150 g) for 10 min. The squeezed BC was then soaked in a beaker with 10 mL of a given solvent and stirred for 2 h at room temperature. Afterward, the soaked BC was briefly drained of excess solvent and placed without pressing in an oven to dry (60 °C, 24 h). Finally, dried BC was carbonized in a tubular furnace under an Ar flow of 100 mL min^{-1} with a ramp of 10 °C min^{-1} to 900 °C and kept there for 1 h.

2.3. Characterization

The water and alcohol-soaked BCs, were tested by Fourier transform infrared spectroscopy with attenuated total reflectance (FTIR-ATR). The measurements were carried out by Spectrophotometer Jasco 4700 equipment. The scan range was 400–4000 cm^{-1}. All scanning electron microscopy (SEM) images were obtained by FEI Quanta 200 FEG-ESEM equipment at 15 kV acceleration voltage, 10 mm working distance. Cross-sections were obtained by dipping samples in liquid nitrogen and then, cutting them with a blade. All samples were placed on an aluminum holder with adhesive carbon tape. For transmission electron microscopy (TEM) analysis, samples were sonicated in ethanol for a few seconds and dropped on carbon-coated copper grids. TEM images were obtained by JEOL JEM1210 TEM with an ORIUS 831 SC 600 (Gatan camera) at 120 kV. N_2 adsorption/desorption measurements were conducted by Micromeritics ASAP 2020 equipment. The outgas conditions were at 120 °C for 12 h. The thermal properties of dried BCs were investigated by a TGA-DSC/DTA analyzer (NETZSCH STA 449 F1 Jupiter). The thermal conditions were 10 °C min^{-1} (ramp), 1000 °C (final temperature) and Ar atmosphere. The X-ray diffraction (XRD) patterns of all samples were performed by Siemens D-5000 equipment with Cu K_α radiation. Tests were carried out in a 2θ range of 10–90°. The crystallinity index (CI) of BCs was calculated by the following equation:

$CI=(I_{110}-I_{am})/I_{110}$ (1) where I_{110} is the intensity of the peak at 22.5° for the crystalline part of cellulose type I and I_{am} is the intensity of the peak at about 18° for the amorphous part [31].

2.4. Electrochemical performance

A slurry was prepared by gently grinding carbon samples in a mortar and mixing with PVDF (8:2 carbon/PVDF w/w) and few drops NMP. The slurry was then casted on a 10 mm diameter carbon paper (Freudenberg H2315). Then, the coated carbon paper was put in a vacuum oven at 80 °C for 24 h to remove NMP. The mass loading of air cathode is about 1 mg cm^{-2}. The Li–O_2 battery is composed of 3 parts, carbon paper, glass fibre filter and Li foil. A 1 M lithium triflate solution in DEGDME was used as the electrolyte. The Li–O_2 batteries were assembled in an Ar filled glove box (H_2O < 0.1 ppm, O_2 < 0.1 ppm). All the tests were carried out in 1 atm dry O_2 to avoid the effect of CO_2 and humidity. The cycle voltammetry measurements were conducted at a scan rate of 20 mV s^{-1} in the range of 2.0–4.5 V (versus Li/Li^+) by a Bio-logic VMP3 multichannel potentiostat. Galvanostatic discharge/charge tests were performed by a battery cycling equipment (MTI BST8-WA).

The estimation of the electrochemical surface area (ECSA) was based on the evaluation of the electrochemical double-layer capacitance and performed in a three-electrode system with a 1 M lithium triflate in DEGDME electrolyte after Ar bubbling. Carbon-coated carbon paper prepared as described above, with a mass loading of about 0.2 mg was used as the working electrode. Platinum wires were used as the counter and the reference electrode. The measurements were conducted at 2 mV s^{-1} in a narrow potential range. The electrochemical double-layer capacitance C_{EDL} was obtained by the following equation [32]:

$$C_{EDL} = \int iVdV/(2\nu m \triangle V) \quad (2)$$

where i is the current, V is the potential, m is the mass of carbons, ν is the scan rate, ΔV is the potential range. The ECSA is given by the [33]:

ECSA = C_{EDL}/C^* (3) where C^* is the specific capacitance (F m^{-2}) of a bare glassy carbon electrode in the same electrolyte. A C^* value of 14.06 μF cm^{-2} was determined by electrochemical impedance spectroscopy (EIS, Fig. S5).

3. Results and discussion

As reported by previous literature [29,30], alcohol treatments contribute to better preserve porous structures in dried cellulose reducing the degree of hornification. We tested several solvents as water replacement of the bacterial cellulose hydrogel, focusing in particular on aliphatic alcohols of different chain lengths, carbonized and tested as electrodes in Li/O_2 batteries. As summarized in Table S1, the poorest results are obtained with water, which seems

to confirm the effect of the high surface tension. Other parameters, such as solvent volatility may also play a role in the pore formation and could help explaining differences between alcohols. To better understand the impact that the replacement of water in the hydrogel for an organic solvent we focused on the characterization of the preparative steps of the carbons obtained from untreated (BC-w), ethanol (BC-e) as a reference alcohol treatment and 1-butanol treated cellulose (BC-b) which present the best electrochemical results. The cleaned, cubic-shaped BC hydrogels were pressed to about 10% of the original height to remove the majority of the entrapped water. Pressed BCs were then soaked in the different alcohols and stirred for 2 h. During this time, the BC cubes swelled to recover more than 90% of the original size in ethanol and more than 70% in the case of 1-butanol. FTIR spectra of soaked BC are similar to those of the pure solvents, which is consistent with complete solvent substitution (Fig. S1a and Figure S1c-d). The alcohol treatment does not chemically alter BCs, according to FTIR spectroscopy of dried BCs (Fig. S1b and Fig. S1c-d). In fact, dried BCs show typical cellulose peaks, which can respectively be ascribed to the stretching vibration of O–H (3350 cm^{-1}), H–C–H (2900 cm^{-1}), C–O–C (1427 cm^{-1}) [34], with no apparent difference between them, which also proves the quantitative solvent removal in the three cases.

The SEM image (Fig. S2) of BC-w shows a smooth surface, which demonstrates that fibrils have compacted. The cross-section SEM images (Fig. 1a–c) show that the layers of BC-w are more densified in comparison with BC-e and BC-b. This confirms that the treatment of ethanol and 1-butanol reduce interfibrillar contraction. The morphology differences between BC-w, BC-e can be attributed to the following factors. On the one hand, the much smaller surface tensions of ethanol and 1-butanol (Table S1), which decrease the capillary force effects as compared to water during the solvent evaporation [29,35]. Low surface tensions of ethanol and 1-butanol result in weaker capillary forces during the process of drying. The fibrils under weak capillary forces move less than under stronger capillary forces resulting from water, barely changing the distance between fibrils. On the other hand, ethanol and 1-butanol can attach to the surface of fibrils via hydrogen-bond [36,37]. As a consequence, the self-association behavior of fibrils can be limited by the steric hindrance of the aliphatic chains of ethanol and 1-butanol, which act as a spacer. Initially weaker and finally repulsive forces will be present among fibrils, preventing their cohesion. Therefore, highly porous structures can be achieved by ethanol and even more by 1-butanol treatment for BC.

The porous structures of dried BCs were further verified by nitrogen adsorption-desorption measurements (Fig. 1d). All three isotherms present hysteresis and could be considered of mixed type II and IV. Pore size distributions (Fig. 1e) mainly range in the mesoporous region, with a macropore contribution in the case of alcohol-treated samples, while micropores are scarce in all three samples. Dried BC-w presents small area and porosity (BET specific surface area 21 $m^2\ g^{-1}$ and cumulative pore volume 0.11 $cm^3\ g^{-1}$, Table 1). In contrast, BC-e and BC-b have respectively over four and five times larger surface areas and pore volumes. These increments agree with the textured structure observed by SEM in BC-e and BC-b. The pore size distributions (Fig. 1e) of all dried BCs are dominated by mesopores, but BC-e and BC-b have larger predominant pore sizes than BC-w.

Powder X-ray diffraction (XRD) was used to study the effect of alcohols on the crystallinity of BCs. Fig. 1g depicts that all BCs show typical pattern peaks (14.5° and 22.5°) of cellulose type I, which correspond to the (100) and (110) lattice planes respectively [39]. Comparing with the crystallinity of BC-w (78%), the crystallinity of BC-e (66%) and BC-b (70%) decreases slightly. The decrease in crystallinity suggests that the cellulose becomes more disordered and loosen, which can be attributed to the effect of dissociation of

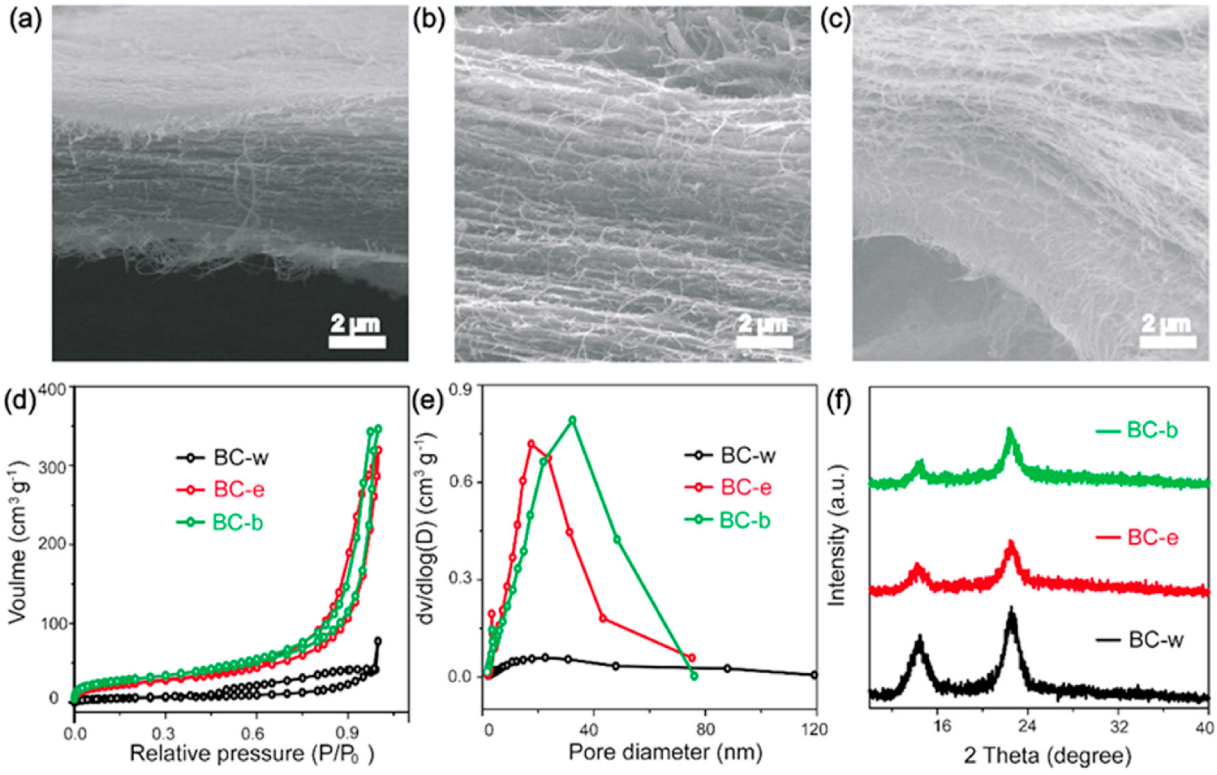

Fig. 1. Characterization of different dried BCs. SEM cross-section images of BC-w (a), BC-e (b) and BC-b (c), nitrogen adsorption–desorption of dried BCs (d), pore size distribution (e), XRD (f).

Table 1
Textural data of samples and the electrochemical surface area (ECSA) of carbons.

Samples	BET surface area ($m^2\ g^{-1}$)	External surface area ($m^2\ g^{-1}$)	Pore Volume ($cm^3\ g^{-1}$)	Predominant pore size (nm)	ECSA ($m^2\ g^{-1}$)
Dried	21	18.29	0.11	14	/
BC-w					
Dried BC-e	88	91.83	0.44	17	/
Dried BC-b	107	102.51	0.54	32	/
Carbon-w	1009	153.44	0.19	16	33
Carbon-e	848	142.26	0.41	27	99
Carbon-b	669	237.42	1.25	85	180
Super P [38]	67	70	0.14	40	115

the hydrogen bonds between cellulose [40].

To explore the effect of the fiber aggregation on the carbonization process, all dried BCs were subjected to Thermogravimetric Analysis (TGA) under Ar (Fig. S3a). There are two major mass losses during the temperature ramp. The first small mass loss step (25–100 °C) can be attributed to the evaporation of residual absorbed water [41]. The loss is larger for BC-w (2.5%) than for alcohol-treated samples (0.9% for BC-e and 0.1% for BC-b). This can be considered a proof that a large part of the most tightly bound water molecules was removed during the alcohol treatment. The second mass loss step occurred at 200–400 °C, corresponding to BC decomposition and carbonization. During this step cellulose depolymerizes and fragments on variable molecular weight forms, giving place to char, tar, and volatile compounds (such as water, carbon dioxide and monoxide, acetic acid, and different saccharides) [42]. The yield of these solid, liquid and gaseous fractions has a strong influence on the subsequent carbonization process. The DSC curves (Fig. S3b) indicated that the temperatures for the first major decomposition peaks of BC-e (286 °C) and BC-b (297 °C) are lower than BC-w (322 °C). This can be related to the lower crystallinity of BC-e and BC-b, which can facilitate the degradation process of BCs [43]. In addition, carbon yields (Fig. S3a) of BC-e (9%) and BC-b (10%) are lower than BC-w (14%), probably because of the smaller pores of BC-w. These smaller pores retain more strongly the pyrolysis liquid intermediates, which are also involved in cross-linking and char formation [44]. The impregnation of a less porous system implies a smaller liquid-gas interface and a stronger liquid-solid interaction, reducing the intermediate volatilization and increasing char production, resulting in a larger carbon yield [42,44].

The presence of liquid intermediates is evident from the textures observed after carbonizing dried BCs at 900 °C in Ar. Carbon originated from water-treated BC (carbon-w) presents a compact vitreous morphology (Fig. 2a), which implies that their pores only correspond to narrow gaps between components of carbon-w. In contrast, carbons derived from ethanol (carbon-e) and 1-butanol (carbon-b) present evident porous structures (Fig. 2b and c), although the original fibrous structure is not retained. The disappearance of fibrous structure probably can be ascribed to the melting of nanofibers during the high temperature treatment. The TEM images of carbons (Fig. S4) show that particularly carbon-b possesses more developed and open porous structures, while carbon-w appears denser than carbon-e and carbon-b. This indicates that ethanol and, particularly, 1-butanol treatments are beneficial to obtain porous carbons from BC. The porous structure properties of carbons were further studied by nitrogen adsorption-desorption measurements (Fig. 2c and Table 1). Although the BET surface area of carbon-w results larger than other carbons, its pore structure mainly consists of micropores (Fig. 2d). Instead, the pore structure of carbon-b is dominated by macropores and mesopores, resulting in a larger external area. Therefore, the more open structure of BC-e and BC-b seems to be beneficial for forming a broader porous structure during pyrolysis. The XRD patterns of carbons are shown in Fig. 2e. The broad peak at around 23° present in the three cases can be attributed to the (002) plane of graphitic carbon [45].

The electrode architecture has a dramatic effect on the discharge capacity of Li–O_2 batteries, as shown by several previous studies [38,46], which are useful to understand the behavior of our materials in this application. Therefore, the electrochemical surface area (ECSA) was determined to gain textural insights from the electrochemical point of view of the porous carbons [47,48], in the same electrolyte used in Li–O_2 battery tests. The values were obtained from capacitive currents in cyclic voltammetry (CV) of the different carbons coated on a carbon paper support (Fig. 3a). The ECSA of bare carbon paper is very small (0.14 $m^2\ g^{-1}$), which means that it has little contribution to the electrochemical interface. The ECSA of carbon-b (180 $m^2\ g^{-1}$) is the largest among the carbons derived from BCs, as carbon-e provided 99 $m^2\ g^{-1}$ and carbon-w 33 $m^2\ g^{-1}$ (Fig. 3b and Table 1). Thus, the largest BET area of BC-w translates into the smallest electrochemically effective area, showing that the smallest micropores are not accessible for our electrolyte, similarly to what we previously demonstrated with ionic liquid electrolytes [46]. Instead, the larger pores of alcohol-treated carbons offer a better ion-accessible surface area, and show larger ECSA values.

ECSA seems a more significant parameter to predict effectiveness as Li–O_2 cathode than BET area. Fig. 3c displays cyclic voltammetry curves of our carbons in O_2 atmosphere at a scan rate of 20 mV s^{-1}. There are one reduction peak and one oxidation peak, which can be respectively ascribed to the formation and the decomposition of Li_2O_2 [49]. Compared with carbon-w, alcohol-treated carbons display higher currents for both reduction and oxidation peaks. This shows that carbon-e and carbon-b provide better oxygen redox activities thanks to their more suitable pore structure. Galvanostatic discharge-charge profiles of Li–O_2 batteries were operated at the current density of 0.1 mA cm^{-2} (Fig. 3d). The contribution of bare carbon fiber support is negligible (Fig. S6). Carbon-b and carbon-e provide discharge capacities of 5.58 and 1.36 mA h cm^{-2}, while carbon-w only gives capacity similar to that of the support alone (0.14 mA h cm^{-2}). Carbon-b also has the highest discharge voltage (~2.75 V), which can be attributed to its larger ECSA. The larger area significantly decreases overpotentials in Li–O_2 batteries and in effect correlation between specific area and discharge potential has been shown previously [38,50]. These capacities clearly show that not only the larger pore volume, but also the larger pore sizes favor the more abundant discharge of Li_2O_2 [51]. The poor capacity of carbon-w can be attributed to its small pore size. This is reflected by the low ECSA and is consistent with our previous observation that only pores larger than a certain size, in the order of 10 nm, significantly contribute to the cathode capacity [46,52]. Besides, small pores will be easily blocked, which hinders the diffusion of oxygen [53]. Instead, the other carbons

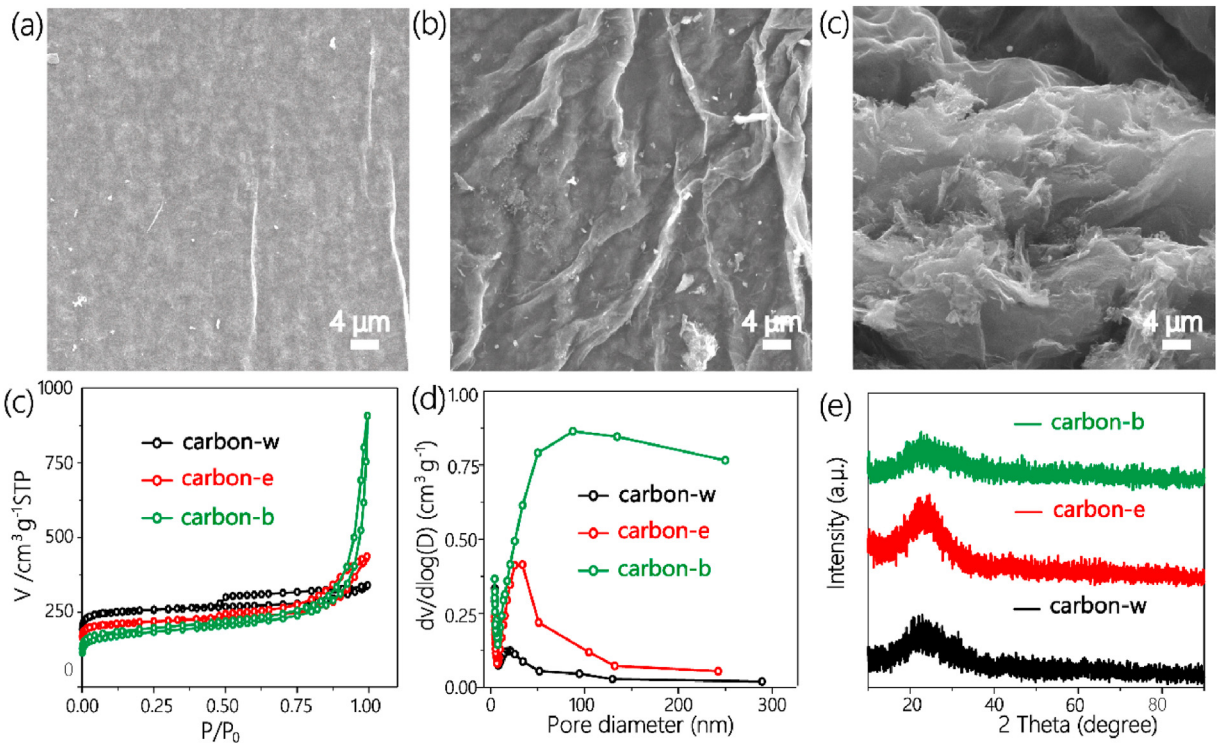

Fig. 2. SEM images of dried carbon-w (a), carbon-e (b) and carbon-b (c), nitrogen adsorption–desorption (c), pore size distribution (d), XRD (e) of carbons obtained from alcohol-treated bacterial cellulose.

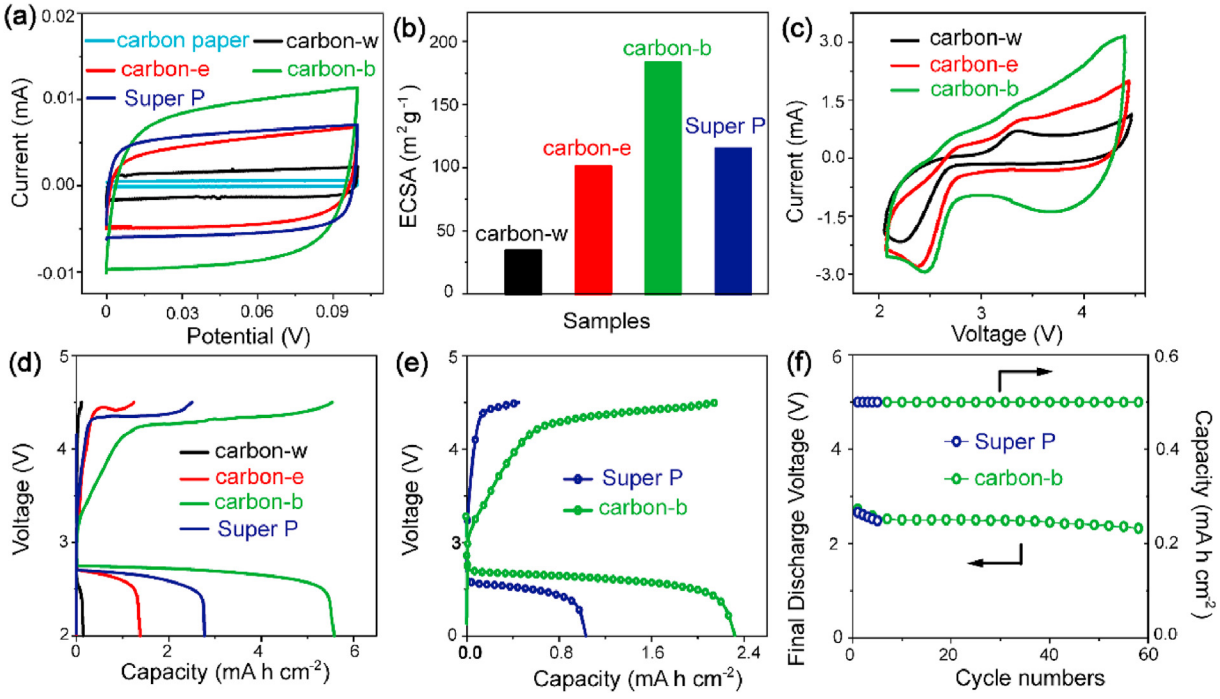

Fig. 3. Electrochemical properties of carbons: (a) CV curves of carbons in Ar-saturated 1 M lithium triflate in DEGDME; (b) comparison of ECSAs; (c) CV curves of Li–O_2 batteries with carbon cathodes; (d) full discharge-charge profiles within the voltage range of 2.0–4.5 V at 0.1 mA cm^{-2}; (e) full discharge-charge profiles at 0.4 mA cm^{-2}; (f) cycle life of carbon-b tested at 0.1 mA cm^{-2}.

show a much more suitable pore structure, in particular carbon-b which outperforms Super P, a carbon black with a very open structure that typically offers large capacity [38,52]. The capacity difference between carbon-b and Super P can be attributed to the different architecture of carbon-b which offers wider pores and larger surface area that allows for a better distribution of discharge products (Table 1 and Table S2). In addition, BC treated with 1-butanol for 24 h showed similar morphologies and discharge

capacities (Fig. S7), confirming that 2 h soaking is sufficient for quantitative water removal. Compared to other reported carbons, carbon-b exhibits outstanding discharge capacity properties as it can be observed in Table S4.

The rate capabilities of carbon-b and Super P cathodes were compared at the increased current density of 0.4 mA cm^{-2} (Fig. 3e). With the increment of the current density, the discharge capacity descended, discharge voltage decreased and charge voltage increased in all cases, but more severely for Super P. This better rate capability can be attributed to larger ECSA, demonstrating again the optimal texture of alcohol-treated carbons as Li–O_2 cathodes. Carbon-b cathodes, displayed nearly 100% coulomb efficiency at 0.1 mA cm^{-2}, and still 90% at 0.4 mA cm^{-2}. However, due to the larger overpotentials, Super P exhibited poorer figures (92% at 0.1 mA cm^{-2}, 43% at 0.4 mA cm^{-2}). In line with this behavior, the cycling stability of carbon-b was far superior to that of Super P. In a test at 0.1 mA cm^{-2} with a capacity limitation of 0.5 mA h cm^{-2} (Fig. 3f and Fig. S8), the Super P electrode only sustained 4 cycles against more than 58 cycles for carbon-b. Table S3 depicts a comparison of the electrochemical performance for several reported cathodes. The outstanding number of cycles that carbon-b can withstand makes it an attractive material for Li–O_2 batteries.

To prove the specificity of the bacterial cellulose texture, cotton linters and agarose were also treated with water and 1-butanol, but the improvement from water to 1-butanol was not large (Fig. S9 and Fig. S10). This can be probably because the fibers of cotton linters and the bulk of agarose are much thicker and densified than the fiber structure of dried BCs. Other alcohols (such as methanol, 1-propanol, 1-hexanol and 1-octanol) and some non-alcohol solvents (acetone, ether and TEGDME) were also used to treat BCs with the same preparation method. All carbons derived from BCs treated with these solvents exhibit better capacities for Li–O_2 batteries than carbon-w (Fig. S11 and Table S1) but lower than carbon-b. This shows that 1-butanol has optimal affinity for cellulose, probably due to its mixed hydrophobic-hydrophilic character [54,55]. However, in general it can be affirmed that the treatment of solvents with low surface tensions on BCs can promote excellent carbons for Li–O_2 batteries.

4. Conclusions

Porous carbons employed as cathodes in Li–O_2 batteries have been successfully synthesized by using alcohols to treat BC. The much higher porosity compared to that of carbon originated from water-treated BC, seems to correspond to the more open structure of the intermediate dried cellulose, even if in all cases the fiber network is lost during carbonization. The structure obtained by treatment of BC with 1-butanol shows optimal properties as a cathode in a Li–O_2 battery, with much higher capacity (5.58 mA h cm^{-2}), lower overpotentials and longer cycling life than the water treated equivalent material. This performance is superior even to a reference commercial cathode material such as Super P, demonstrating a clear interest as a practical material for application in metal-air batteries, as well as metal-sulphur, supercapacitors and all systems that require efficient transport properties.

CRediT authorship contribution statement

Wenhai Wang: Conceptualization, Methodology, Investigation, Formal analysis, Writing – original draft. **Siavash Khabazian:** Methodology. **Soledad Roig-Sanchez:** Methodology, Writing – review & editing. **Anna Laromaine:** Writing – review & editing. **Anna Roig:** Writing – review & editing. **Dino Tonti:** Resources, Conceptualization, Writing – review & editing, Supervision.

Declaration of competing interest

The authors declare that they have no known competing financial interests or personal relationships that could have appeared to influence the work reported in this paper.

Acknowledgments

This research was supported by the Spanish Government, through the “Severo Ochoa” Programme for Centers of Excellence in R&D (CEX2019-000917-S), the projects MAT2017-91404-EXP and RTI2018-096273-B-I00 and the PhD scholarships of S. R. (BES-2016-077533) with FEDER co-funding. W.W. gratefully acknowledges the support from the China Scholarship Council (CSC No.:201808340076). The authors participate in the SusPlast and FLOWBAT 2021 platforms promoted by the Spanish National Research Council (CSIC) and in the Aerogels COST ACTION (CA 18125). They also acknowledge the Generalitat de Catalunya (2017SGR765 and 2017SGR1687 grants). This work has been performed within the framework of the doctoral program in materials science of UAB (W. W. and S.R–S.)

Appendix B. Supplementary data

Supplementary data to this article can be found online at https://doi.org/10.1016/j.renene.2021.05.059.

References

[1] C. Xia, C.Y. Kwok, L.F. Nazar, A high-energy-density lithium-oxygen battery based on a reversible four-electron conversion to lithium oxide, Science 361 (2018) 777–781.
[2] P. Salimi, O. Norouzi, S.E.M. Pourhoseini, P. Bartocci, A. Tavasoli, F. Di Maria, S.M. Pirbazari, G. Bidini, F. Fantozzi, Magnetic biochar obtained through catalytic pyrolysis of macroalgae: a promising anode material for Li-ion batteries, Renew. Energy 140 (2019) 704–714.
[3] J.J. Xu, Q.C. Liu, Y. Yu, J. Wang, J.M. Yan, X.B. Zhang, In situ construction of stable tissue-directed/reinforced bifunctional separator/protection film on lithium anode for lithium-oxygen batteries, Adv. Mater. 29 (24) (2017) 1606552.
[4] E. Wang, S. Dey, T. Liu, S. Menkin, C.P. Grey, Effects of atmospheric gases on Li metal cyclability and solid-electrolyte interphase formation, ACS Energy Lett 5 (4) (2020) 1088–1094.
[5] Y. Qiao, Q. Wang, X. Mu, H. Deng, P. He, J. Yu, H. Zhou, Advanced hybrid electrolyte Li-O_2 battery realized by dual superlyophobic membrane, Joule 3 (12) (2019) 2986–3001.
[6] C.M. Burke, R. Black, I.R. Kochetkov, V. Giordani, D. Addison, L.F. Nazar, B.D. McCloskey, Implications of 4 e^- oxygen reduction via iodide redox mediation in Li–O_2 batteries, ACS Energy Lett 1 (4) (2016) 747–756.
[7] I. Landa-Medrano, I. Lozano, N. Ortiz-Vitoriano, I. Ruiz de Larramendi, T. Rojo, Redox mediators: a shuttle to efficacy in metal–O_2 batteries, J. Mater. Chem. A. 7 (2019) 8746–8764.
[8] J. Lu, Y.J. Lee, X. Luo, K.C. Lau, M. Asadi, H.H. Wang, S. Brombosz, J. Wen, D. Zhai, Z. Chen, D.J. Miller, Y.S. Jeong, J.B. Park, Z.Z. Fang, B. Kumar, A. Salehi-Khojin, Y.K. Sun, L.A. Curtiss, K. Amine, A lithium-oxygen battery based on lithium superoxide, Nature 529 (7586) (2016) 377–382.
[9] W.J. Kwak, Rosy, D. Sharon, C. Xia, H. Kim, L.R. Johnson, P.G. Bruce, L.F. Nazar, Y.K. Sun, A.A. Frimer, M. Noked, S.A. Freunberger, D. Aurbach, Lithium-oxygen batteries and related systems: potential, status, and future, Chem. Rev. 120 (2020) 6626–6683.
[10] M. Olivares-Marín, P. Palomino, J.M. Amarilla, E. Enciso, D. Tonti, Effects of architecture on the electrochemistry of binder-free inverse opal carbons as Li–air cathodes in an ionic liquid-based electrolyte, J. Mater. Chem. A. 1 (45) (2013) 14270–14279.
[11] L. Ma, T. Yu, E. Tzoganakis, K. Amine, T. Wu, Z. Chen, J. Lu, Fundamental understanding and material challenges in rechargeable nonaqueous Li-O_2 batteries: recent progress and perspective, Adv. Energy Mater. 8 (22) (2018) 1800348.
[12] D.M. Itkis, D.A. Semenenko, E.Y. Kataev, A.I. Belova, V.S. Neudachina, A.P. Sirotina, M. Havecker, D. Teschner, A. Knop-Gericke, P. Dudin, A. Barinov, E.A. Goodilin, Y. Shao-Horn, L.V. Yashina, Reactivity of carbon in lithium-oxygen battery positive electrodes, Nano Lett. 13 (10) (2013) 4697–4701.
[13] M. Kim, E. Yoo, W.-S. Ahn, S.E. Shim, Controlling porosity of porous carbon cathode for lithium oxygen batteries: influence of micro and meso porosity, J. Power Sources 389 (2018) 20–27.
[14] S. Roig-Sanchez, E. Jungstedt, I. Anton-Sales, D.C. Malaspina, J. Faraudo,

L.A. Berglund, A. Laromaine, A. Roig, Nanocellulose films with multiple functional nanoparticles in confined spatial distribution, Nanoscale Horiz 4 (3) (2019) 634–641.
[15] A. Alonso-Díaz, J. Floriach-Clark, J. Fuentes, M. Capellades, N.S. Coll, A. Laromaine, Enhancing localized pesticide action through plant foliage by silver-cellulose hybrid patches, ACS Biomater. Sci. Eng. 5 (2) (2019) 413–419.
[16] G. Fei, Y. Wang, H. Wang, Y. Ma, Q. Guo, W. Huang, D. Yang, Y. Shao, Y. Ni, Fabrication of bacterial cellulose/polyaniline nanocomposite paper with excellent conductivity, strength, and flexibility, ACS Sustain. Chem. Eng. 7 (9) (2019) 8215–8225.
[17] D. Abol-Fotouh, B. Dorling, O. Zapata-Arteaga, X. Rodriguez-Martinez, A. Gomez, J.S. Reparaz, A. Laromaine, A. Roig, M. Campoy-Quiles, Farming thermoelectric paper, Energy Environ. Sci. 12 (2) (2019) 716–726.
[18] X. Hao, J. Wang, B. Ding, Y. Wang, Z. Chang, H. Dou, X. Zhang, Bacterial-cellulose-derived interconnected meso-microporous carbon nanofiber networks as binder-free electrodes for high-performance supercapacitors, J. Power Sources 352 (2017) 34–41.
[19] L. Zuo, W. Fan, Y. Zhang, Y. Huang, W. Gao, T. Liu, Bacterial cellulose-based sheet-like carbon aerogels for the in situ growth of nickel sulfide as high performance electrode materials for asymmetric supercapacitors, Nanoscale 9 (13) (2017) 4445–4455.
[20] E. Jazaeri, L. Zhang, X. Wang, T. Tsuzuki, Fabrication of carbon nanofiber by pyrolysis of freeze-dried cellulose nanofiber, Cellulose 18 (6) (2011) 1481–1485.
[21] N. Pircher, L. Carbajal, C. Schimper, M. Bacher, H. Rennhofer, J.M. Nedelec, H.C. Lichtenegger, T. Rosenau, F. Liebner, Impact of selected solvent systems on the pore and solid structure of cellulose aerogels, Cellulose 23 (3) (2016) 1949–1966.
[22] Y. Peng, D.J. Gardner, Y. Han, Drying cellulose nanofibrils: in search of a suitable method, Cellulose 19 (1) (2011) 91–102.
[23] A.A. Alhwaige, H. Ishida, S. Qutubuddin, Carbon aerogels with excellent CO2 adsorption capacity synthesized from clay-reinforced biobased chitosan-polybenzoxazine nanocomposites, ACS Sustain. Chem. Eng. 4 (3) (2016) 1286–1295.
[24] Y. Li, Y. Liu, M. Wang, X. Xu, T. Lu, C.Q. Sun, L. Pan, Phosphorus-doped 3D carbon nanofiber aerogels derived from bacterial-cellulose for highly-efficient capacitive deionization, Carbon 130 (2018) 377–383.
[25] D.Y. Chung, Y.J. Son, J.M. Yoo, J.S. Kang, C.Y. Ahn, S. Park, Y.E. Sung, Coffee waste-derived hierarchical porous carbon as a highly active and durable electrocatalyst for electrochemical energy applications, ACS Appl. Mater. Interfaces 9 (47) (2017) 41303–41313.
[26] C. Wang, D. Wu, H. Wang, Z. Gao, F. Xu, K. Jiang, A green and scalable route to yield porous carbon sheets from biomass for supercapacitors with high capacity, J. Mater. Chem. A. 6 (3) (2018) 1244–1254.
[27] L. Hu, Q. Zhu, Q. Wu, D. Li, Z. An, B. Xu, Natural biomass-derived hierarchical porous carbon synthesized by an in situ hard template coupled with NaOH activation for ultrahigh rate supercapacitors, ACS Sustain. Chem. Eng. 6 (11) (2018) 13949–13959.
[28] L. Zhang, T. You, T. Zhou, X. Zhou, F. Xu, Interconnected hierarchical porous carbon from lignin-derived byproducts of bioethanol production for ultra-high performance supercapacitors, ACS Appl. Mater. Interfaces 8 (22) (2016) 13918–13925.
[29] A. Tejado, W.C. Chen, M.N. Alam, T.G.M. van de Ven, Superhydrophobic foam-like cellulose made of hydrophobized cellulose fibres, Cellulose 21 (2014) 1735–1743.
[30] J. Li, T. Song, H. Xiu, M. Zhang, R. Cheng, Q. Liu, X. Zhang, E. Kozliak, Y. Ji, Foam materials with controllable pore structure prepared from nanofibrillated cellulose with addition of alcohols, Ind. Crop. Prod. 125 (2018) 314–322.
[31] E. Alonso, M. Faria, F. Mohammadkazemi, M. Resnik, A. Ferreira, N. Cordeiro, Conductive bacterial cellulose-polyaniline blends: influence of the matrix and synthesis conditions, Carbohydr. Polym. 183 (2018) 254–262.
[32] L. Zhang, H. Gong, Improvement in flexibility and volumetric performance for supercapacitor application and the effect of Ni–Fe ratio on electrode behaviour, J. Mater. Chem. A. 3 (14) (2015) 7607–7615.
[33] H. Peng, B. Yao, X. Wei, T. Liu, T. Kou, P. Xiao, Y. Zhang, Y. Li, Pore and heteroatom engineered carbon foams for supercapacitors, Adv. Energy Mater. 9 (19) (2019) 1803665.
[34] H. Zhang, X. Sun, M.A. Hubbe, L. Pal, Highly conductive carbon nanotubes and flexible cellulose nanofibers composite membranes with semi-interpenetrating networks structure, Carbohydr. Polym. 222 (2019) 115013.
[35] Z. Hanif, H. Jeon, T.H. Tran, J. Jegal, S.-A. Park, S.-M. Kim, J. Park, S.Y. Hwang, D.X. Oh, Butanol-mediated oven-drying of nanocellulose with enhanced dehydration rate and aqueous re-dispersion, J. Polym. Res. 24 (3) (2017) 191–201.
[36] Z. Lu, Z. Su, S. Song, Y. Zhao, S. Ma, M. Zhang, Toward high-performance fibrillated cellulose-based air filter via constructing spider-web-like structure with the aid of TBA during freeze-drying process, Cellulose 25 (1) (2017) 619–629.
[37] J. Juntaro, S. Ummartyotin, M. Sain, H. Manuspiya, Bacterial cellulose reinforced polyurethane-based resin nanocomposite: a study of how ethanol and processing pressure affect physical, mechanical and dielectric properties, Carbohydr. Polym. 87 (4) (2012) 2464–2469.
[38] M. Olivares-Marín, M. Aklalouch, D. Tonti, Combined influence of meso- and macroporosity of soft-hard templated carbon electrodes on the performance of Li-O_2 cells with different configurations, Nanomaterials 9 (6) (2019) 810–822.
[39] M. Zeng, A. Laromaine, A. Roig, Bacterial cellulose films: influence of bacterial strain and drying route on film properties, Cellulose 21 (6) (2014) 4455–4469.
[40] H. Chen, J. Chen, N. Teng, H. Na, J. Zhu, Controlling the status of corn cellulose solutions by ethanol to define fiber morphology during electrospinning, Cellulose 24 (2) (2016) 863–870.
[41] L. Wang, M. Ago, M. Borghei, A. Ishaq, A.C. Papageorgiou, M. Lundahl, O.J. Rojas, Conductive carbon microfibers derived from wet-spun lignin/nanocellulose hydrogels, ACS Sustain. Chem. Eng. 7 (6) (2019) 6013–6022.
[42] Z. Wang, B. Pecha, R.J.M. Westerhof, S.R.A. Kersten, C.-Z. Li, A.G. McDonald, M. Garcia-Perez, Effect of cellulose crystallinity on solid/liquid phase reactions responsible for the formation of carbonaceous residues during pyrolysis, Ind. Eng. Chem. Res. 53 (8) (2014) 2940–2955.
[43] Z. Wang, A.G. McDonald, R.J.M. Westerhof, S.R.A. Kersten, C.M. Cuba-Torres, S. Ha, B. Pecha, M. Garcia-Perez, Effect of cellulose crystallinity on the formation of a liquid intermediate and on product distribution during pyrolysis, J. Anal. Appl. Pyrol. 100 (2013) 56–66.
[44] P.C. Lewellen, W.A. Peters, J.B. Howard, Cellulose pyrolysis kinetics and char formation mechanism, Symp. (Int.) Combust. 16 (1) (1977) 1471–1480.
[45] P.P. Ghimire, M. Gao, M. Jaroniec, Amino acid-assisted synthesis of porous graphitic carbon spheres with highly dispersed Ni nanoparticles, Carbon 153 (2019) 206–216.
[46] M. Olivares-Marín, P. Palomino, E. Enciso, D. Tonti, Simple method to relate experimental pore size distribution and discharge capacity in cathodes for Li/O_2 batteries, J. Phys. Chem. C 118 (36) (2014) 20772–20783.
[47] H. Wang, J. Wang, Y. Pi, Q. Shao, Y. Tan, X. Huang, Double perovskite $LaFe_xNi_{1-x}O_3$ nanorods enable efficient oxygen evolution electrocatalysis, Angew. Chem. Int. Ed. 58 (8) (2019) 2316–2320.
[48] S.D. Ghadge, O.I. Velikokhatnyi, M.K. Datta, P.M. Shanthi, S. Tan, K. Damodaran, P.N. Kumta, Experimental and theoretical validation of high efficiency and robust electrocatalytic response of one-dimensional (1D) $(Mn,Ir)O_2$:10F nanorods for the oxygen evolution reaction in PEM-based water electrolysis, ACS Catal. 9 (3) (2019) 2134–2157.
[49] P. Wang, C. Li, S. Dong, X. Ge, P. Zhang, X. Miao, Z. Zhang, C. Wang, L. Yin, One-step route synthesized Co_2P/Ru/N-doped carbon nanotube hybrids as bifunctional electrocatalysts for high-performance Li-O_2 batteries, Small 15 (30) (2019) 1900001.
[50] K.-H. Xue, T.-K. Nguyen, A.A. Franco, Impact of the cathode microstructure on the discharge performance of lithium air batteries: a multiscale model, J. Electrochem. Soc. 161 (8) (2014) E3028–E3035.
[51] M. Benoit, A. Rodrigues, K. De Oliveira Vigier, E. Fourré, J. Barrault, J.-M. Tatibouët, F. Jérôme, Combination of ball-milling and non-thermal atmospheric plasma as physical treatments for the saccharification of microcrystalline cellulose, Green Chem. 14 (8) (2012) 2212–2215.
[52] M. Aklalouch, M. Olivares-Marin, R.C. Lee, P. Palomino, E. Enciso, D. Tonti, Mass-transport control on the discharge mechanism in Li-O_2 batteries using carbon cathodes with varied porosity, ChemSusChem 8 (20) (2015) 3465–3471.
[53] N. Ding, S.W. Chien, T.S.A. Hor, R. Lum, Y. Zong, Z. Liu, Influence of carbon pore size on the discharge capacity of Li–O_2 batteries, J. Mater. Chem. 2 (31) (2014) 12433–12441.
[54] H.-M. Kao, C.-C. Cheng, C.-C. Ting, L.-Y. Hwang, Phase control of cubic SBA-1 mesostructures via alcohol-assisted synthesis, J. Mater. Chem. 15 (29) (2005) 2989–2992.
[55] C. Calero, J. Faraudo, D. Bastos-Gonzalez, Interaction of monovalent ions with hydrophobic and hydrophilic colloids: charge inversion and ionic specificity, J. Am. Chem. Soc. 133 (38) (2011) 15025–15035.